Chapter 5

Mechanical Validation

In this chapter the FV implementation of the segregated and whole displacement field algorithms are applied to a variety of validation problems and compared with a standard FE implementation. The problems comprise of applications where analytical, semi-analytical or experimental reference solutions are available, in order to validate the algorithms employed. It should be noted that due to the non-linear nature of the applications under investigation, purely analytical reference solutions are generally not available.

The algorithms are compared with regard to accuracy and computational cost. They are also analysed for a variety of meshes with varying connectivities and element assemblies. The algorithms are compared for two and three dimensional test cases. Complete descriptions of the validation problems will be presented, and the reference solutions will be fully described when possible.

5.1 Test case 1: Uniaxial tensile piece

The first test case is a uniaxial tensile piece undergoing strain hardening. As the problem is uniaxial, a one dimensional analytical solution is available. The application can be modelled in two and three dimensions. The two dimensional approximation is achieved via a plane

stress approximation. Initially, this problem provides a reasonable test case for a variety of elements and element assemblies, orthogonal and non-orthogonal.

For a plane stress approximation the problem is specified in Figure 5.2. In this case, the problem was modelled using a series of orthogonal meshes involving BLQ elements. The mesh was refined in order to investigate the CPU time required for the different algorithmic approaches and associated solvers.

5.1.1 Analytical solution

Assuming a basic one dimensional elasto-visco-plastic model as described in Figure 5.1a, it is possible to derive the following first order ordinary differential equation defining the relationship between a constant applied stress and a time dependent strain under visco-plastic conditions [72]:

$$\gamma \beta \epsilon + \frac{\mathrm{d}\epsilon}{\mathrm{d}t} = \frac{\gamma \beta}{E} \sigma_A + \gamma \left(\sigma_A - Y \right),$$

where σ_A represents the constant applied stress and β is the strain hardening portion of the stress-strain curve after the removal of the elastic strain component, as defined earlier in equation 2.8. The variables γ and Y are the previously defined fluidity and yield stress.
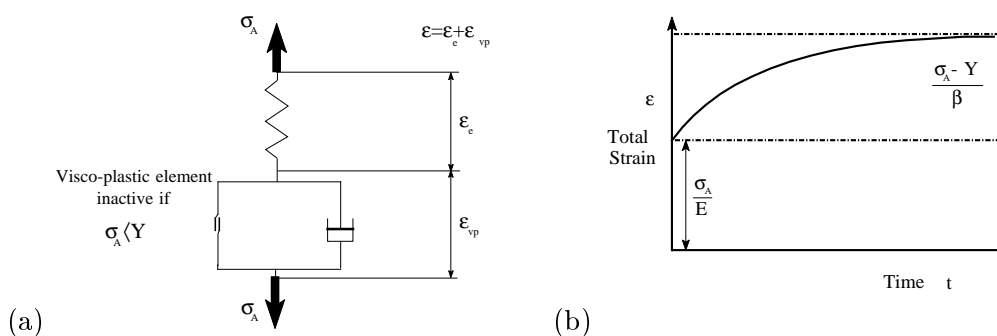

Figure 5.1: One dimensional elasto-visco-plastic (a) model and (b) response.

The solution to the above differential equation is relatively straight forward and is stated

here as
$$\epsilon = \frac{\sigma_A}{E} + \frac{(\sigma_A - Y)}{\beta}\left[1 - e^{-\beta\gamma t}\right].$$

Provided that β is non-zero, the form of response is illustrated in Figure 5.1b which represents an initial elastic response followed by a time dependent strain increase which approaches a steady state value in an exponential fashion.

Hence, the total strain is
$$\epsilon = \frac{\sigma_A}{E} + \frac{(\sigma_A - Y)}{\beta} = \epsilon_e + \epsilon_{vp} \tag{5.1}$$
in the limit $t \to \infty$. It is important to note that the final solution in this limit is independent of the fluidity γ. Hence, the final solution is equivalent to an elasto-plastic analysis. For a time independent solution the time stepping scheme and the fluidity are viewed purely as acceleration parameters in the non-linear solution approach [105].

E	ν	H	Y	γ
$7000\,\mathrm{kgmm}^{-2}$	0.2	$225\,\mathrm{kgmm}^{-2}$	$24.3\,\mathrm{kgmm}^{-2}$	$1.0 \times 10^{-5}\,\mathrm{s}^{-1}$

Table 5.1: Material properties of aluminium alloy 57S.

Considering a tensile piece of aluminium with material properties as described in Table 5.1 and linear strain hardening characteristics as described in section 2.2.3, the strain response to an applied stress σ_A can be obtained from equation 5.1 and is stated in Table 5.2.

σ_A	ϵ	ϵ_{vp}
$27\,\mathrm{kgmm}^{-2}$	1.54714×10^{-2}	1.16143×10^{-2}

Table 5.2: Analytical solution of the strain response to an applied stress.

5.1.2 Numerical solutions

The numerical results for a variety of single elements and simple element assemblies, in two and three dimensions, are described in Tables 5.3 and 5.4. A simple element assembly involving two CST elements is illustrated in Figure 5.2. Equivalent element configurations
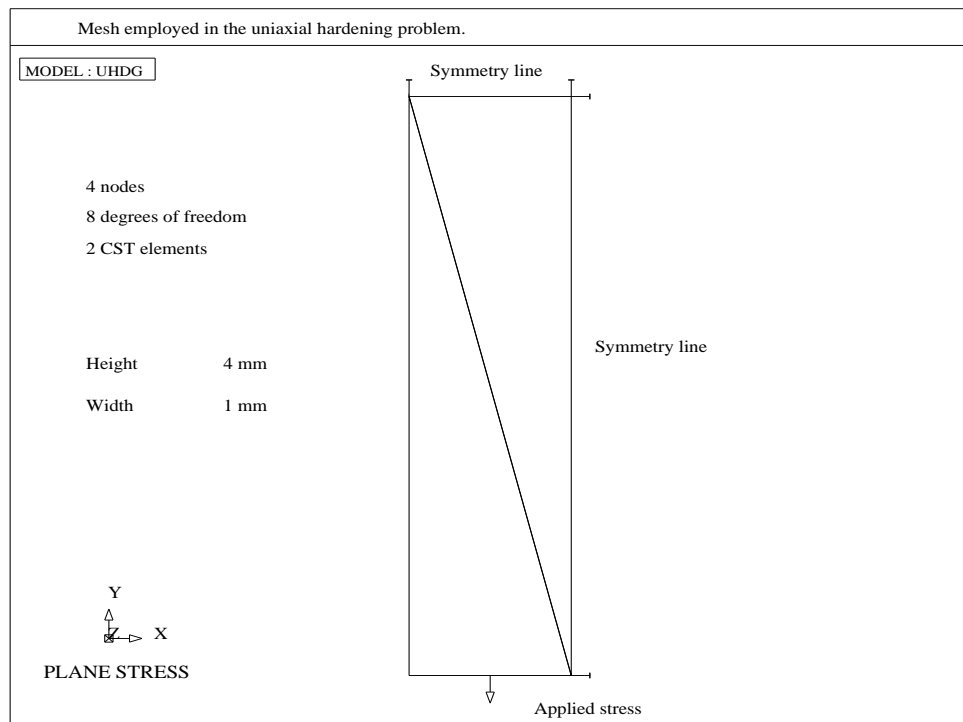
Figure 5.2: Uniaxial hardening problem.

for the FVM and the FEM have been compared. For this validation problem the FVM and the FEM provide complete agreement with regard to the numerical solution, for all elements and element assemblies as described in Tables 5.3 and 5.4. The numerical solution obtained is in good agreement with the analytical solution as stated in Table 5.2.

As described in Tables 5.3 and 5.4 the FEM and the FVM require an equivalent number of time steps to converge. This illustrates the agreement of the two methods with regard to strain response over time.

It should be noted that when the BLQ, TLH or BLP elements are non-orthogonal in the FVM a BiCG (Bi-Conjugate Gradient) solver is employed. The BiCG solver is required as the resultant coefficient matrix is asymmetric. Alternatively, a CGM (Conjugate Gradient Method) solver is always employed in the FEM as the resultant coefficient matrix is always symmetric regardless of the orthogonality of the elements. Additionally, a CGM solver is

	Solver	Time steps	ϵ	ϵ_{vp}
1 BLQ FVM	CGM	232	1.54703×10^{-2}	1.16132×10^{-2}
2 CST FVM	CGM	232	1.54703×10^{-2}	1.16132×10^{-2}
3 BLQ FVM	BiCG	232	1.54703×10^{-2}	1.16132×10^{-2}
1 BLQ FEM	CGM	232	1.54703×10^{-2}	1.16132×10^{-2}
2 CST FEM	CGM	232	1.54703×10^{-2}	1.16132×10^{-2}
3 BLQ FEM	CGM	232	1.54703×10^{-2}	1.16132×10^{-2}

Table 5.3: Numerical results for a plane stress approximation.

	Solver	Time steps	ϵ	ϵ_{vp}
1 TLH FVM	CGM	232	1.54703×10^{-2}	1.16132×10^{-2}
2 BLP FVM	CGM	232	1.54703×10^{-2}	1.16132×10^{-2}
6 LT FVM	CGM	232	1.54703×10^{-2}	1.16132×10^{-2}
3 TLH FVM	BiCG	232	1.54703×10^{-2}	1.16132×10^{-2}
1 TLH FEM	CGM	232	1.54703×10^{-2}	1.16132×10^{-2}
2 BLP FEM	CGM	232	1.54703×10^{-2}	1.16132×10^{-2}
6 LT FVM	CGM	232	1.54703×10^{-2}	1.16132×10^{-2}
3 TLH FEM	CGM	232	1.54703×10^{-2}	1.16132×10^{-2}

Table 5.4: Numerical results for a three dimensional analysis.

employed for both the FEM and the FVM with regard to CST and LT elements. These observations agree with the theoretical discussions of the previous chapter.

This problem furnishes comprehensive patch tests for simple element assemblies and was employed to verify the implementation of the pressure loads with regard to both the FEM and the FVM. This was achieved by applying the pressured load over faces of the element assemblies consisting of non-orthogonal faces. The results were in agreement with those in Table 5.4.

This validation problem is somewhat limited due to the constant values of the stress and strains throughout the tensile piece. Hence, the complete agreement for both methods regardless of element choice. The following mechanical validation problems are more demanding and will provide a more detailed comparison of the two methods.

5.1.3 Algorithm performance

This validation problem was solved using a plane stress approximation with an increasing number of BLQ elements. The FVM using a segregated algorithmic approach and the FVM and the FEM using the standard algorithmic approach, were compared with regard to computational cost. As the BLQ elements can be assembled in an orthogonal fashion for this problem, the CGM solver can be employed for the FVM and the FEM. The CPU time
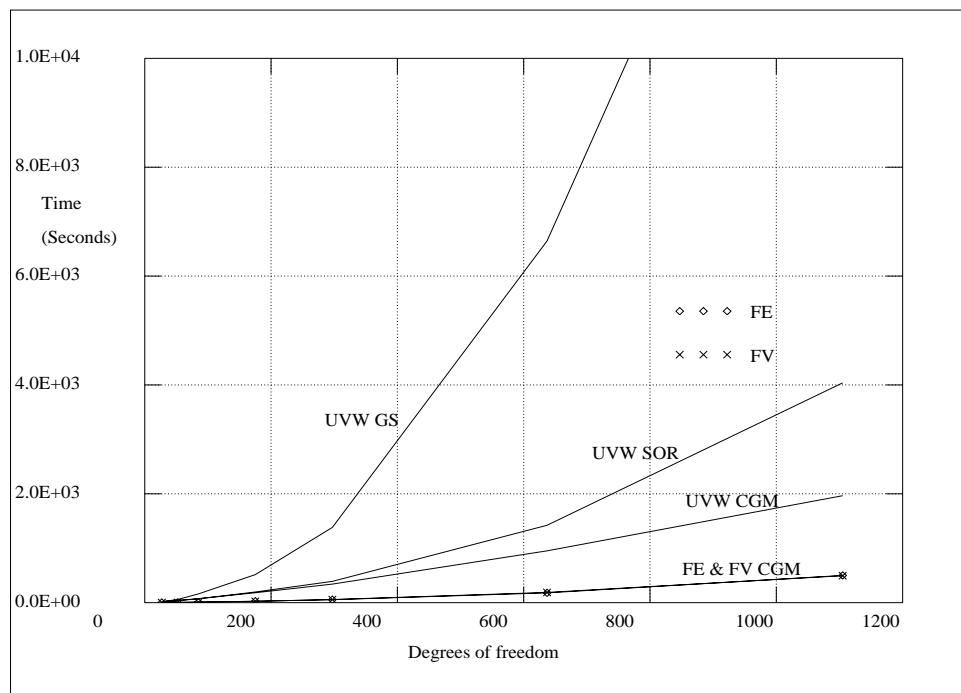

Figure 5.3: CPU times measured on an Intel 486DX 33Mhz processor.

was measured on an Intel 486DX 33MHz processor and the results obtained are plotted in Figure 5.3.

As expected the segregated algorithm (UVW) performs considerably slower than the whole field (FE & FV) algorithms, this is in agreement with the performance of the algorithms when applied to linear elastic problems [43, 42, 4]. The segregated algorithm was studied for a variety of linear solvers. The conjugate gradient solver with Jacobi preconditioning (UVW CGM) performed best, with the SOR solver (UVW SOR) comparing reasonably

well on this simple test case with an over-relaxation factor of $\omega = 1.8$. The Gauss-Seidel solver (UVW GS) showed the poorest performance.

5.2 Test case 2: Perforated tensile strip

The perforated tensile strip has been modelled extensively using the traditional FEM [105, 108] and a reference solution based upon experimental data is available [91]. The problem involves an applied stress as described in Figure 5.4, which is increased incrementally, with the initial increment loading the strip to the yield point and the following load increments causing plastic deformation up to the point of plastic flow. The six applied load increments are described in Table 5.5 For the reference solution the material under investigation was the aluminium alloy 57s as described in the previous validation problem, the properties of which are described in Table 5.1.

	I	II	III	IV	V	VI
Increment (kgmm^{-2})	5.59	0.95	1.46	1.73	1.52	1.64
Total (kgmm^{-2})	5.59	6.54	8.00	9.73	11.25	12.89

Table 5.5: Load increments applied to the perforated tensile strip.

5.2.1 Reference solution

The reference solution with regard to the stress distribution is based upon the experimental results for the total strain. The total strain was measured using a birefringent coating technique on the perforated tensile strip [91]. The stresses were obtained by applying the incremental Prandtl-Reuss stress-strain relations [50]. The total strain and stress profiles obtained along the minimum section of the perforated tensile strip, which is the line X-X' in Figure 5.4, are described for all load increments in Figures 5.5.3 and 5.6.3 respectively.

5.2.2 Numerical analysis

The perforated tensile strip can be modelled using a plane stress approximation, as described in Figure 5.4. The geometry of this problem requires a non-orthogonal mesh with regard to BLQ elements as also illustrated in Figure 5.4. The problem can also be modelled in two dimensions using CST elements. The FVM and the FEM are compared for meshes consisting of BLQ and CST elements.
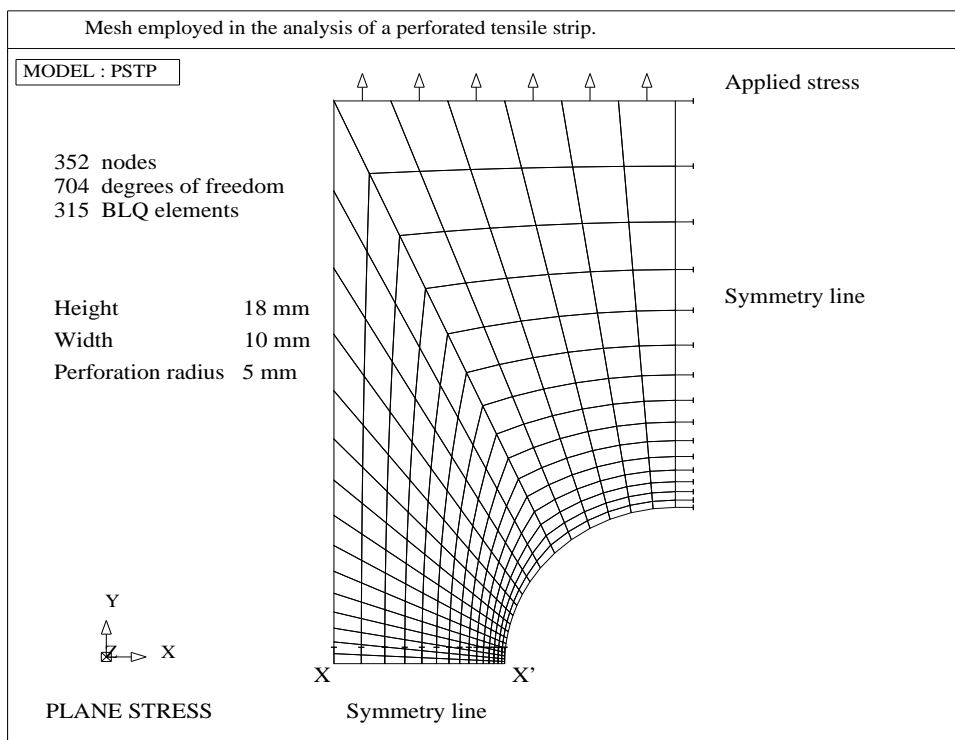

Figure 5.4: Perforated tensile strip

5.2.2.1 Reference numerical analyses

The elasto-visco-plastic solution of this problem is time independent. Hence, the final solution is equivalent to the solution obtained in an elasto-plastic analysis [105]. An elasto-plastic numerical analysis with a Von-Mises yield criterion has been performed using the

commercial engineering software ANSYS [88], in order to provide a further reference solution. An identical mesh, using BLQ elements as described in Figure 5.4, was processed in ANSYS. The total strain profile obtained using ANSYS is described in Figure 5.5.4.

Additionally, an explicit elasto-visco-plastic analysis with a Von-Mises yield criterion has been performed using the commercial engineering software MICROFIELD [81]. Unfortunately, the relevant module in MICROFIELD is restricted to higher order BBQ (Bi-Quadratic Quadrilateral) elements. Hence, an equivalently accurate, but coarser mesh, was processed in MICROFIELD. The stress profile obtained using MICROFIELD is described in Figure 5.6.4.

5.2.3 Discussion of numerical results

With regard to the total strain profile, the previous numerical analyses performed using the FEM, have largely over predicted the strain values when compared to the reference solution [105]. The same over prediction occurs in the numerical analyses performed in this research using the FEM and the FVM, as illustrated in Figures 5.5.1 and 5.5.2 respectively. Relatively good agreement between the numerical analyses and the reference solution is obtained with regard to the stress profile, as illustrated in Figure 5.6.

The problem was modelled with a number of meshes consisting of BLQ and CST elements, with varying mesh density. As predicted from the theoretical analysis in the previous chapter, the results for the FVM and the FEM with regard to CST elements are in complete agreement, as illustrated in Figures 5.8 and 5.10. Hence, providing further evidence to establish the direct equivalence of the two methods with regard to CST elements.

For BLQ elements, the two methods are generally in close agreement, but it is interesting to note that the two methods agree more closely when the problem is loaded initially than at the the final load increment VI, as illustrated in Figures 5.7 and 5.9. At the final load increment the tensile piece is undergoing total strains of several percent, and the infinitesimal strain theory is reaching the limit of applicability. At this stage plastic flow is beginning to occur and the material non-linearity would begin to be augmented

by geometrical non-linearity. Interestingly, the two methods appear to differ more as the overall non-linearity of the problem increases.

5.2.4   Algorithmic performance

For this validation problem, the non-orthogonality of the mesh with regard to BLQ elements requires a BiCG solver for the asymmetric coefficient matrix assembled by the FVM, where as the symmetric coefficient matrix assembled by the FEM requires a CGM solver.

The computational expense of the BiCG solver with regard to the FVM when compared to the FEM is illustrated in Figure 5.11, where the computational processing time is plotted against mesh density. As expected the FVM is approximately twice as expensive as the FEM, because the BiCG solver is computationally twice as expensive as the CGM solver. In this research the Jacobi pre-conditioner is applied for the BiCG and the CGM solver, though it should be noted that a number of other pre-conditioners could be applied that may reduce the computational cost.

For the previous validation problem an orthogonal mesh was employed for BLQ elements and it was possible to employ a CGM solver for the FVM and the FEM, hence the agreement in computational cost as indicated in Figure 5.3.

For meshes consisting of CST elements the coefficient matrices with regard to the FEM and the FVM are identical, hence the CGM solver can be employed for both methods. The computational cost of the FVM and the FEM are in closer agreement as illustrated in Figure 5.12. The FVM is approximately ten percent slower than the FEM, this is attributable to the larger number of integration points associated with the FVM than with the FEM for CST elements, as described in section 4.1.2.1.

5.2.5   Invariant and integration point scheme

In the FVM and the FEM it is necessary to compute and store the constitutive values, such as stress and strain, for all elements. The values can either be calculated and stored at the element centre and assumed invariant over the element or be calculated and stored at the integration points. The latter technique is obviously more accurate, but also requires more storage.

It should be noted that the scheme adopted is not an issue with regard to linear elements as the constitutive values are invariant over the element. The following comparisons are for a mesh consisting of BLQ elements as illustrated in Figure 5.4.

Comparisons of the stress and strain profiles furnished by the invariant and integration point schemes are illustrated in Figures 5.15 and 5.13 and Figures 5.16 and 5.14, for the FVM and the FEM, respectively. A comparison of the integration point scheme for the FVM and the FEM is illustrated in Figures 5.17 and 5.18. The stress and strain profiles are consistent with the invariant schemes employed in the previous numerical analyses, hence the invariant method provides a reasonable solution approach for this problem with a considerable reduction in memory requirements. This can be very important when considering problems involving complex three dimensional geometries, with many thousands of elements.
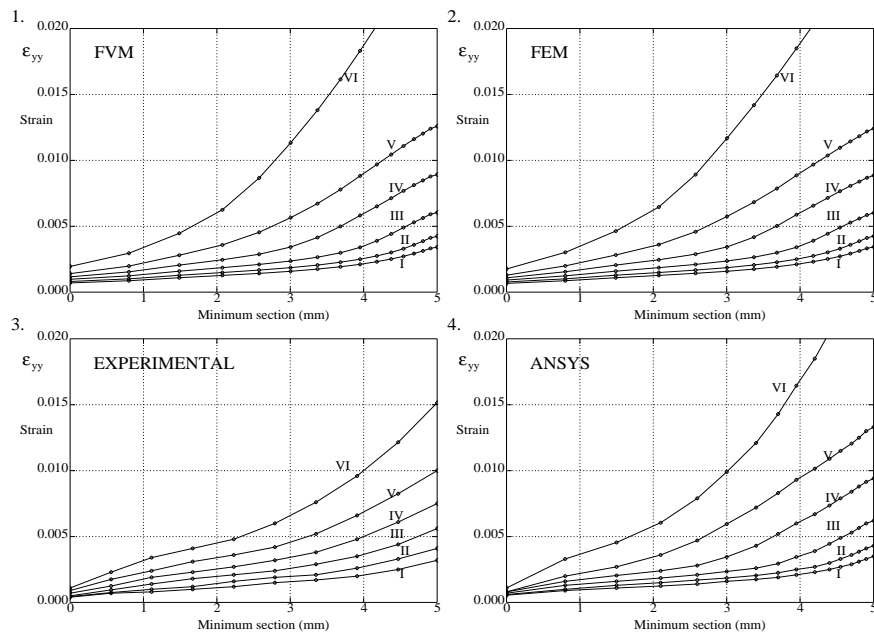
Figure 5.5: Total strain profile of numerical and semi-experimental analyses.
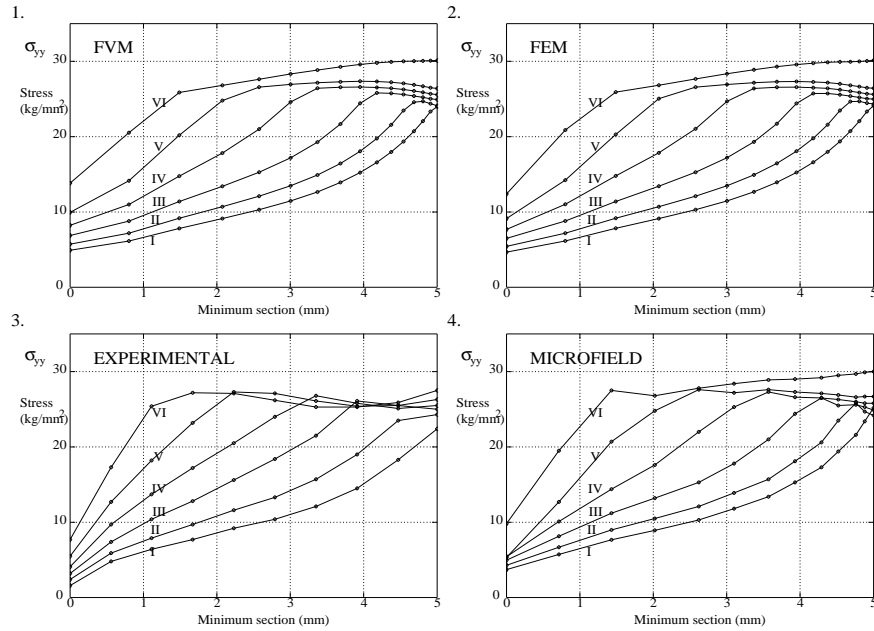
Figure 5.6: Stress profile of numerical and semi-experimental analyses.
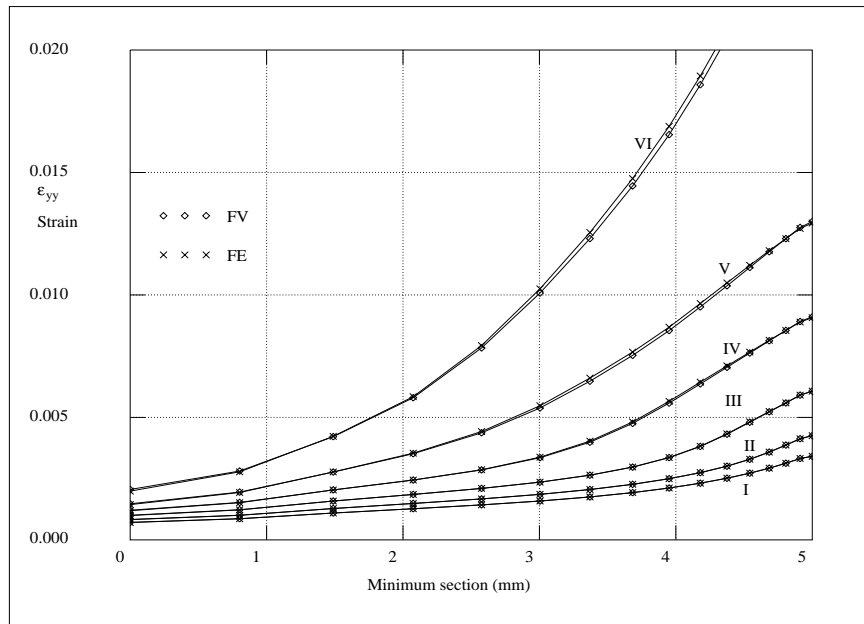
Figure 5.7: Comparison of the total strain for BLQ elements.
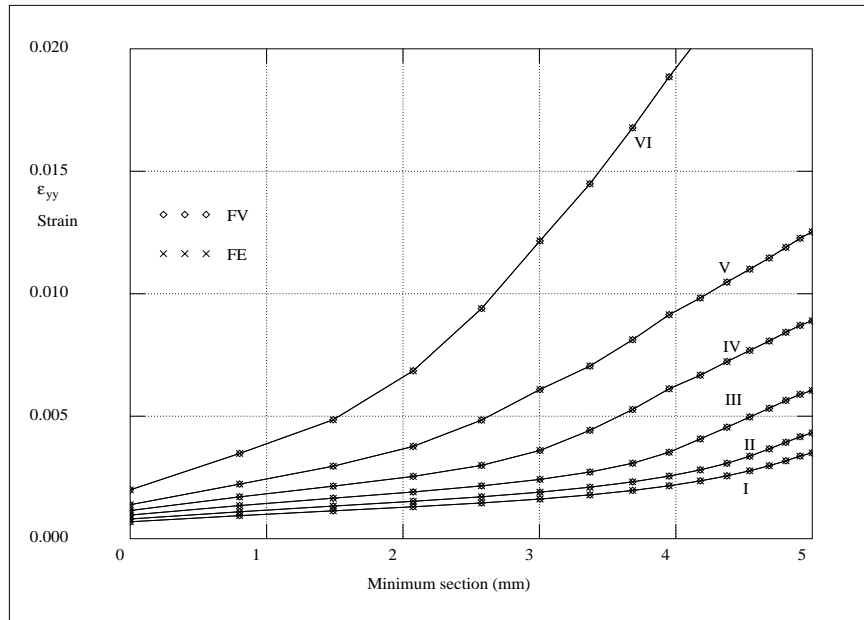
Figure 5.8: Comparison of the total strain for CST elements.
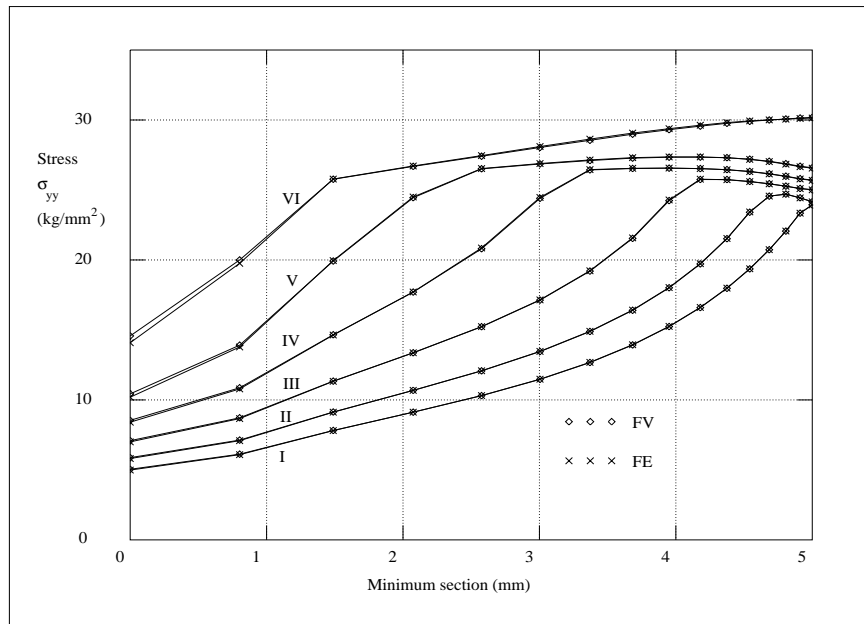
Figure 5.9: Comparison of the stress distribution for BLQ elements.
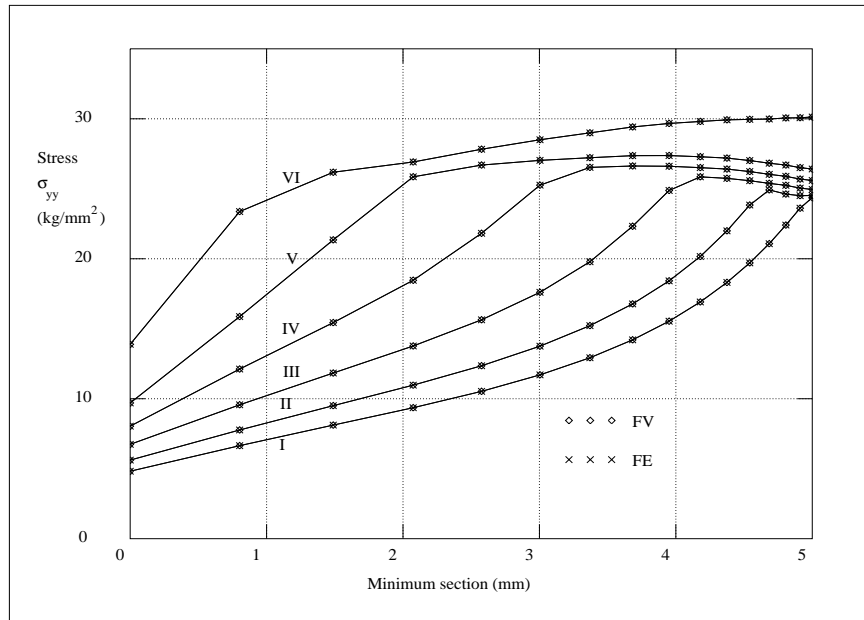
Figure 5.10: Comparison of the stress distribution for CST elements.
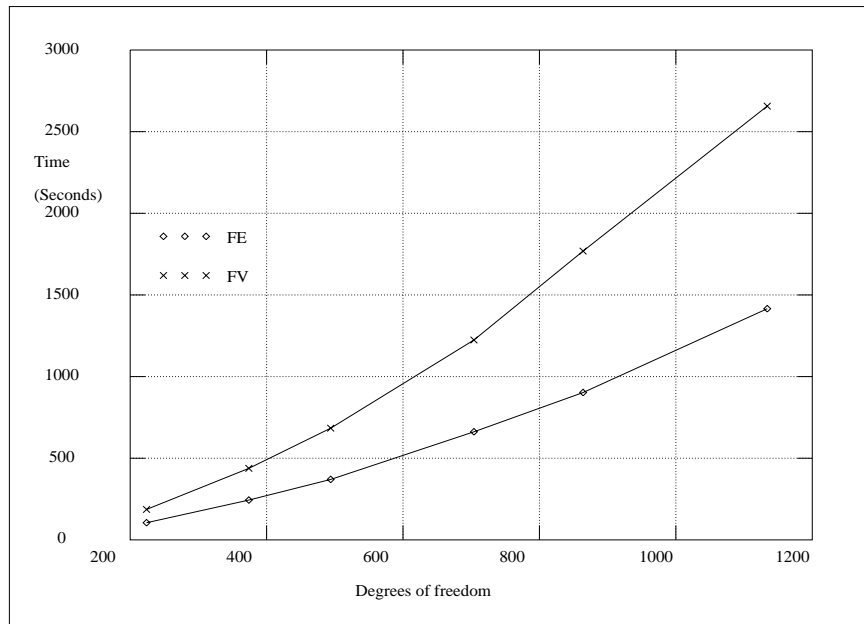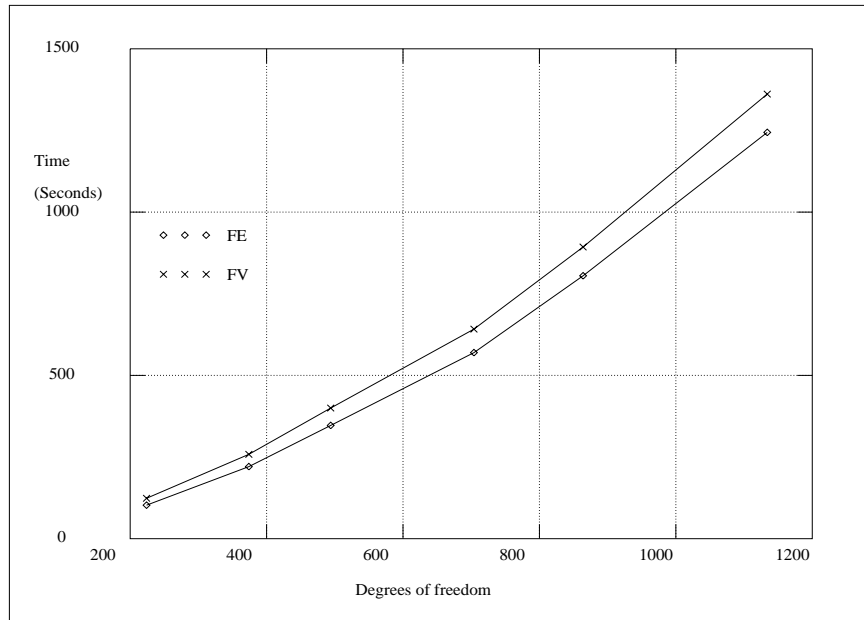
Figure 5.11: CPU times for BLQ elements on a SPARC 4, 110MHz work station.

Figure 5.12: CPU times for CST elements on a SPARC 4, 110MHz work station.
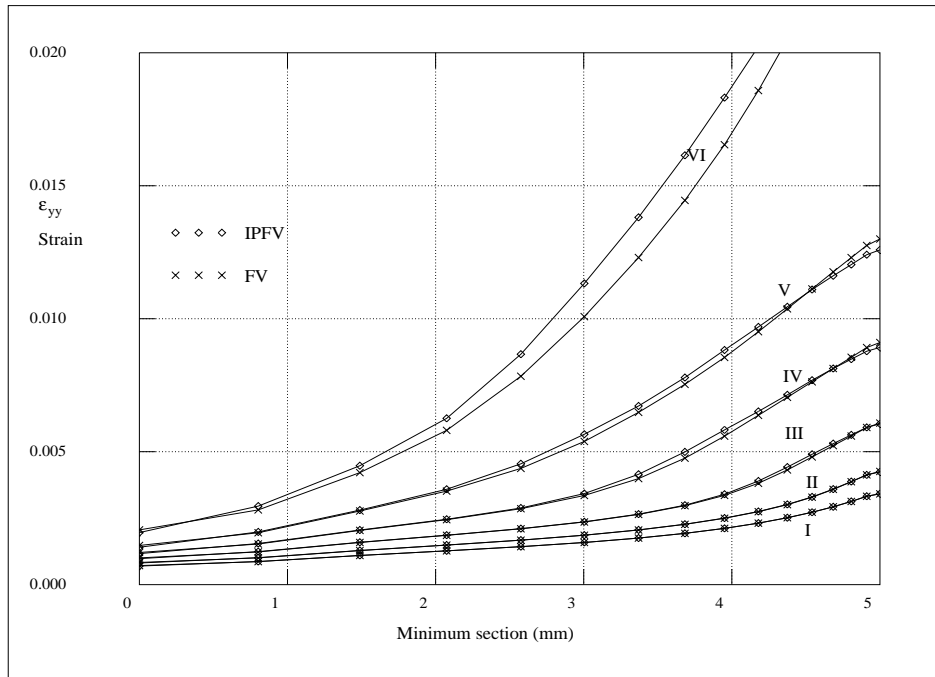
Figure 5.13: Comparison with FV integration point method for strain.
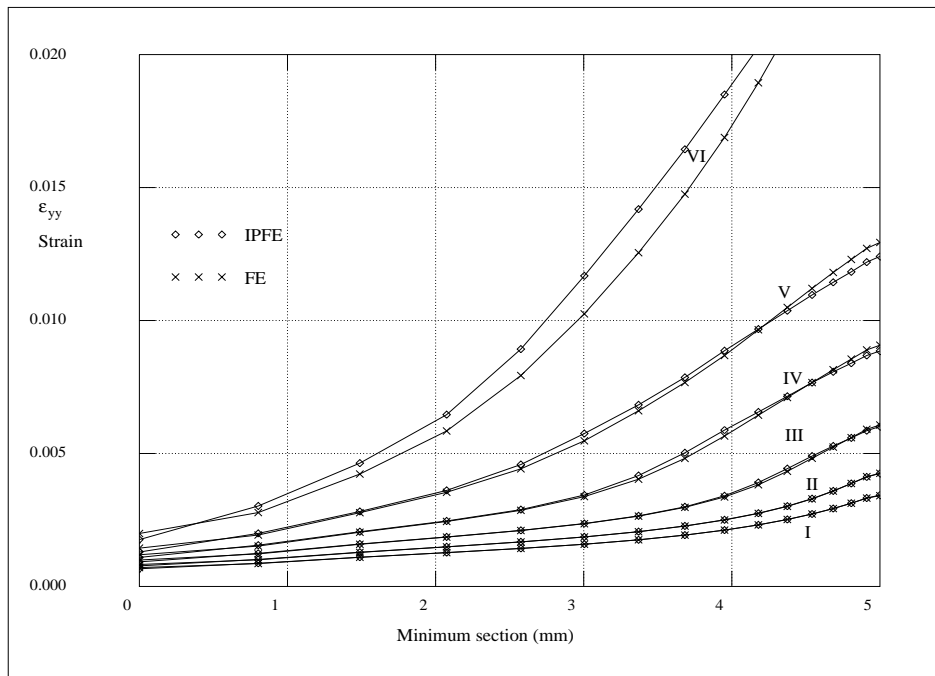
Figure 5.14: Comparison with FE integration point method for strain.
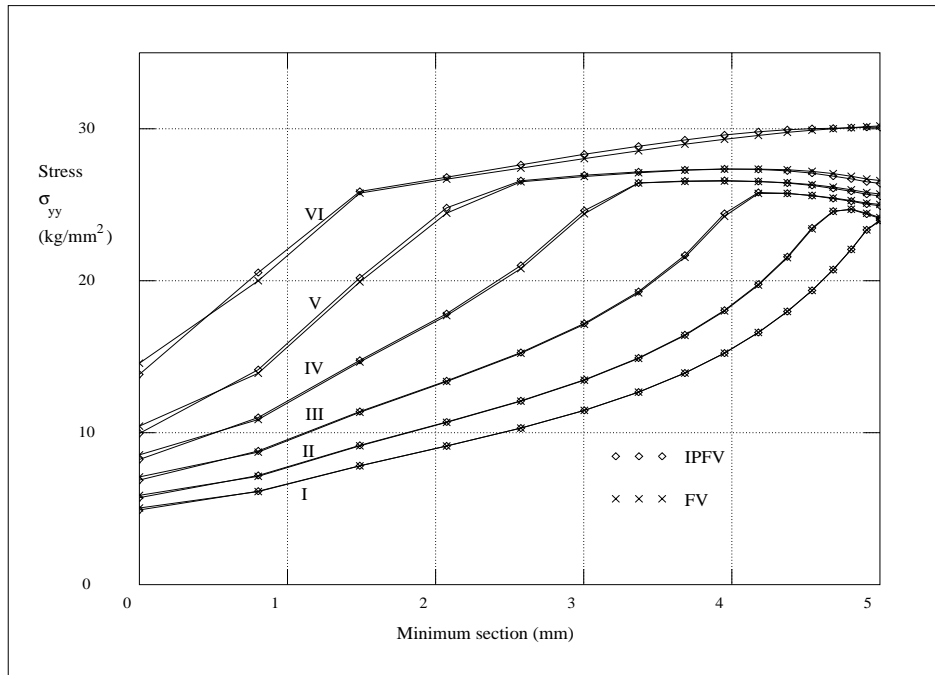
Figure 5.15: Comparison with FV integration point method for stress.
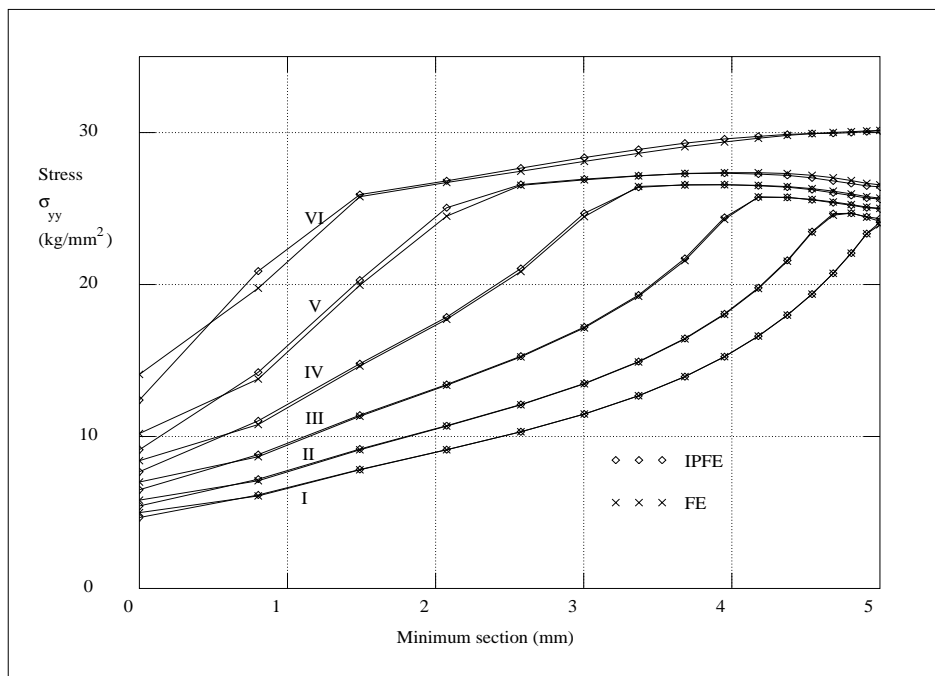
Figure 5.16: Comparison with FE integration point method for stress.
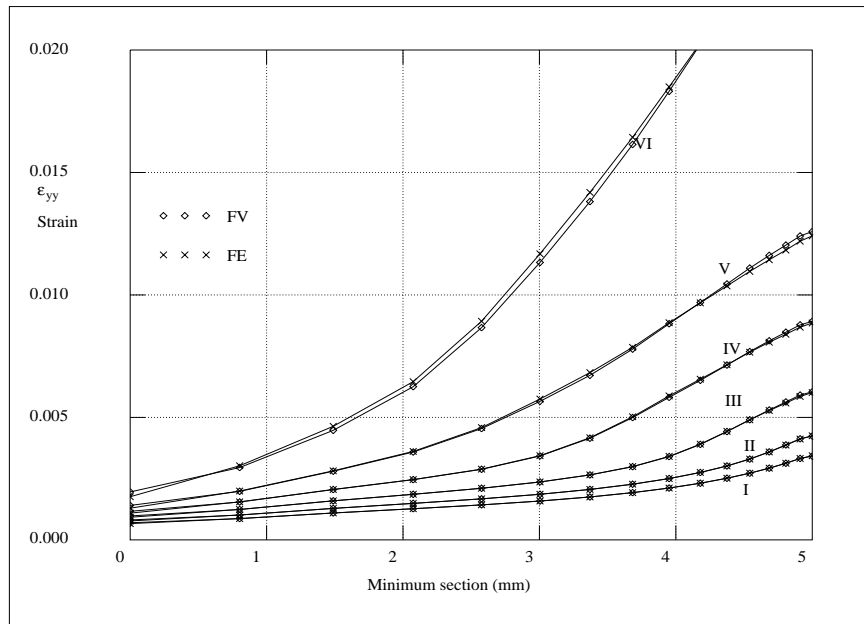
Figure 5.17: Comparison of integration point methods for strain.
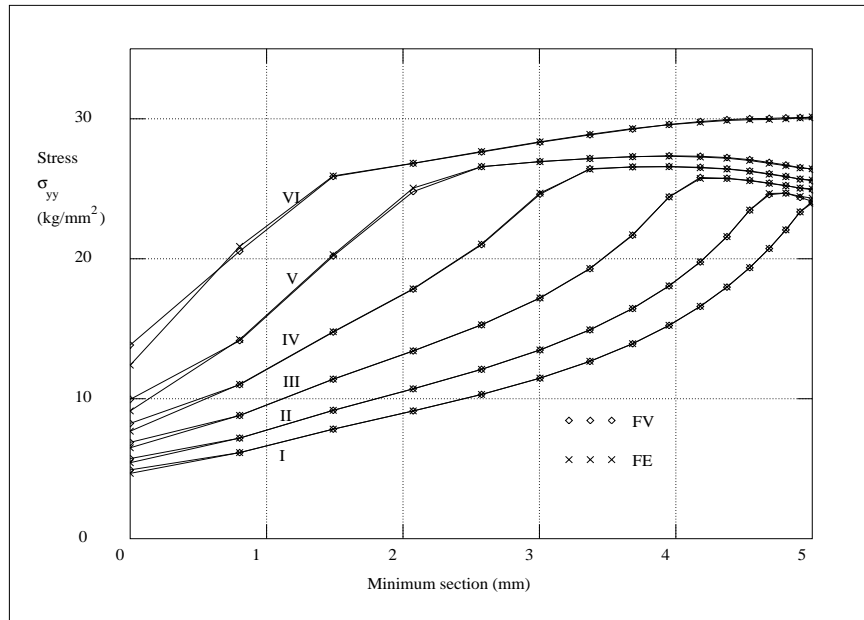
Figure 5.18: Comparison of integration point methods for stress.

5.3 Test case 3: Internally pressurised thick cylinder

For this validation problem a thick walled cylinder consisting of an elastic/perfectly plastic material undergoes an incrementally increasing internal pressure. A Von-Mises yield criterion is associated with the idealized material of the cylinder. The properties of the cylinder material are described in Table 5.6 and the pressure load increments are described in Table 5.7.

E	ν	H	Y	γ
$21000\,\mathrm{dNmm}^{-2}$	0.3	$0\,\mathrm{dNmm}^{-2}$	$24\,\mathrm{dNmm}^{-2}$	$1.0 \times 10^{-5}\,\mathrm{s}^{-1}$

Table 5.6: Material properties of the thick cylinder.

	I	II	III	IV	V	VI	VII
Increment (dNmm^{-2})	8.0	2.0	2.0	2.0	2.0	2.0	2.0
Total (dNmm^{-2})	8.0	10.0	12.0	14.0	16.0	18.0	20.0

Table 5.7: Load increments applied to the pressurized thick cylinder.

5.3.1 Theoretical analysis

As the problem is axisymmetric, a semi-analytical reference solution is available for this validation problem [53]. Due to the non-linear nature of the problem a closed form solution is not available. In the reference solution a hyperbolic system of three quasi-linear first order partial differential equations is obtained, which is then solved numerically after applying a finite difference approximation [53].

5.3.2 Numerical analysis

This problem is also time independent and again the final solution is equivalent to that of an elasto-plastic analysis. An elasto-plastic analysis with a Von-Mises yield criterion has been performed using the commercial engineering software LUSAS [36], in order to provide a

reference numerical solution. The mesh consisting of BLQ elements as described in Figure 5.19 was processed in LUSAS. Numerically the problem can be modelled using a plane
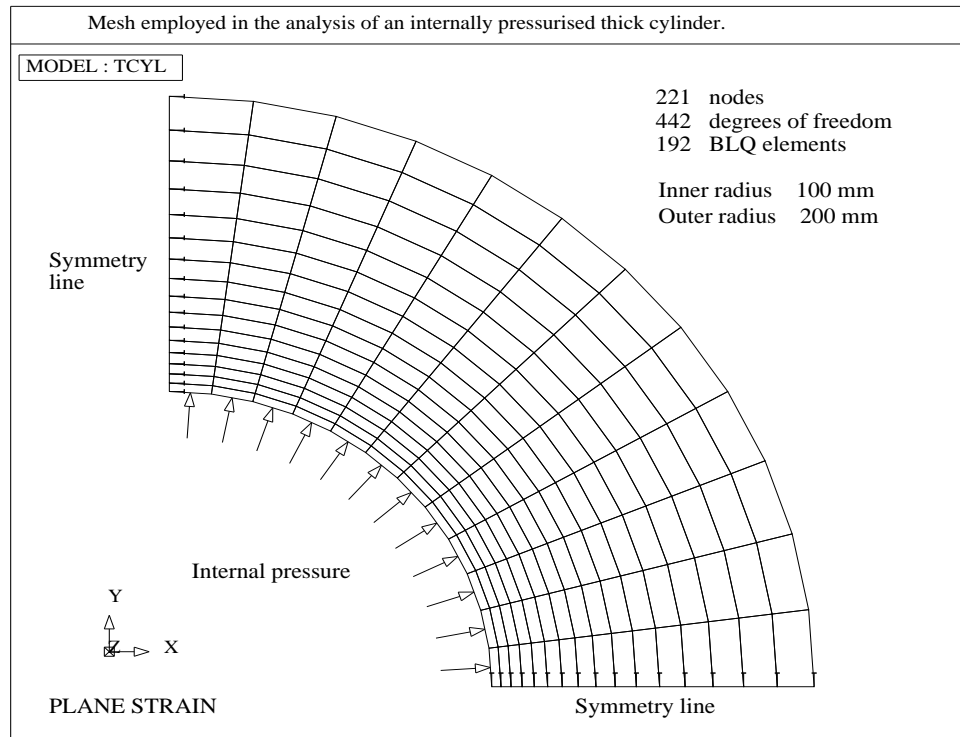

Figure 5.19: Internally pressurized thick cylinder.

strain approximation [72]. The BLQ mesh employed in the numerical analyses performed in this research is also illustrated in Figure 5.19. A mesh consisting of CST elements is also considered.

5.3.3 Discussion of numerical results

For this problem the FEM and the FVM are in very close agreement for both BLQ and CST elements, as indicated by Figures 5.20 and 5.21 respectively. Though it is possible to observe a slight difference between the FVM and the FEM with regard to BLQ elements as the amount of plastic straining increases. Where as for CST elements the two methods are in complete agreement as expected. This is illustrated in Figures 5.22 and 5.23, where

the hoop stresses along the radial axes are compared for the load increment VI, involving an internal pressure of 18dNmm^{-2}.
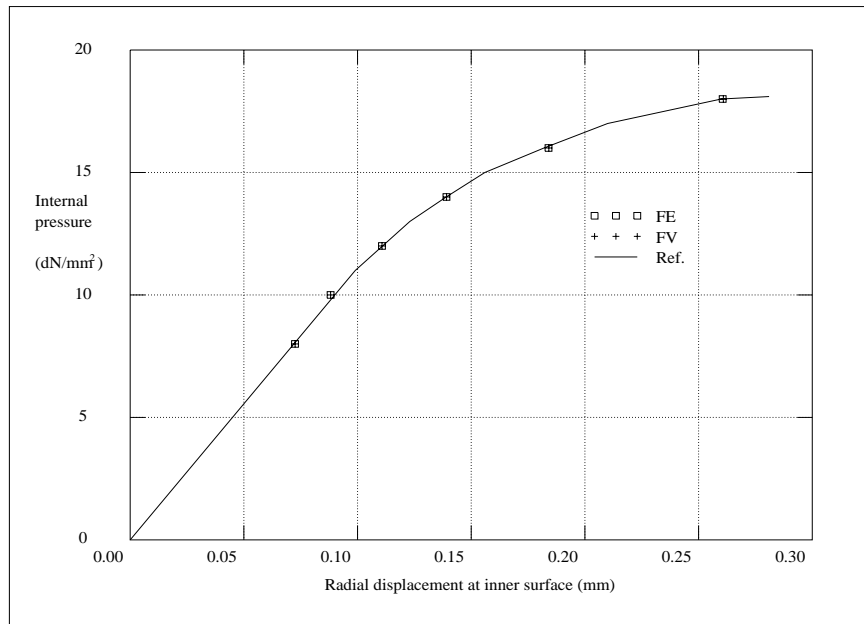
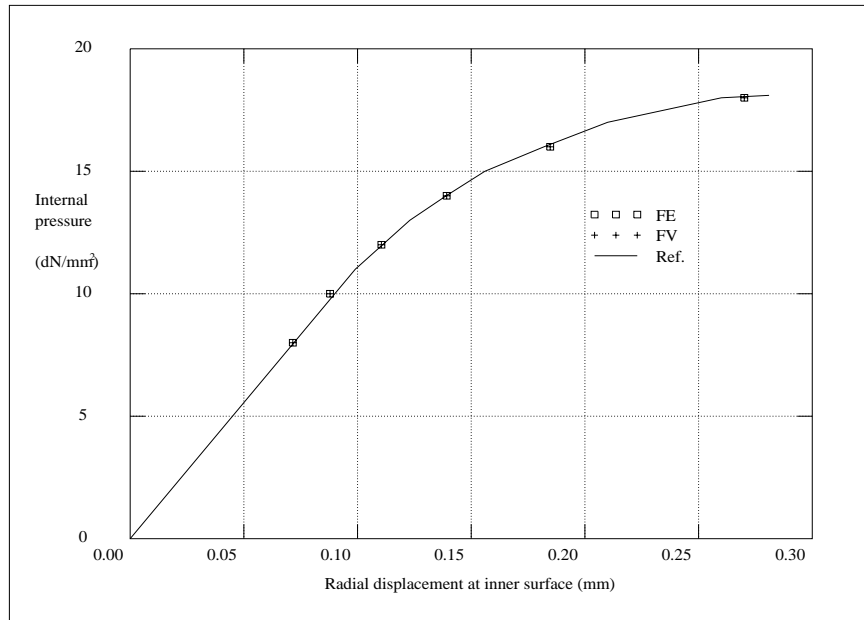Figure 5.20: Mesh consisting of BLQ elements.

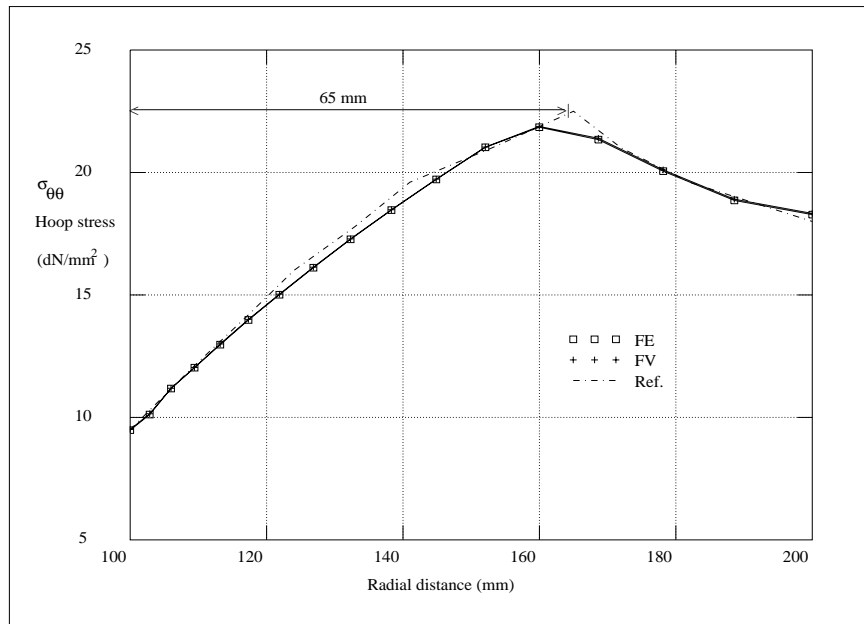Figure 5.21: Mesh consisting of CST elements.
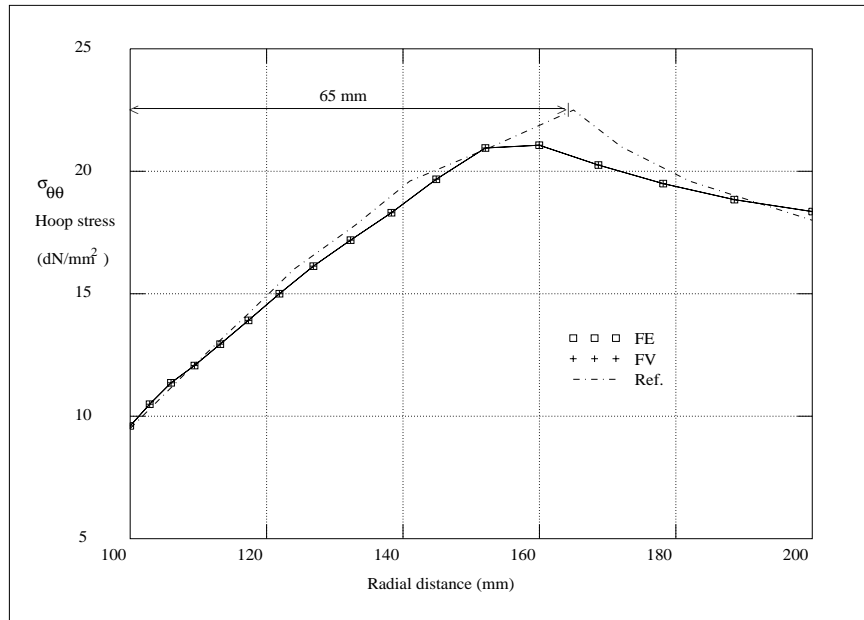
Figure 5.22: Mesh consisting of BLQ elements.

Figure 5.23: Mesh consisting of CST elements.

5.4   Test case 4: Internally pressurised spherical vessel

For this validation problem a thick walled spherical vessel, consisting of an elastic/perfectly plastic material, undergoes an instantaneously applied internal pressure load. A Von-Mises yield criterion is associated with the idealized material of the spherical vessel. The properties of the spherical vessel are equivalent to those of the previous validation problem, which are described in Table 5.6, and the instantaneously applied pressure load is 30dNmm^{-2}.

5.4.1   Theoretical analysis

As the problem is spherical and the pressure load is applied instantaneously, a closed form solution is available [50]. The analytically derived equations will be stated here for completeness. Considering a cross-section through the central point of a hollow sphere, with
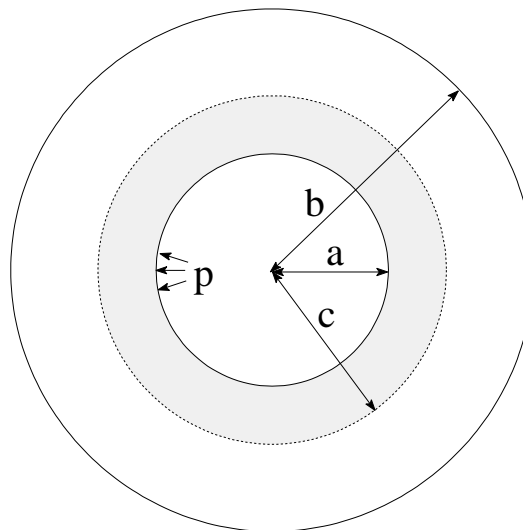

Figure 5.24: Plastic region round a spherical cavity, expanded by a uniformly distributed pressure.

internal radius a and external radius b, as illustrated in Figure 5.24, then the radius of the plastic region c, as a result of the uniformly distributed pressure load p, can be obtained

from solution of

$$\frac{2Y}{3}\left(1 - \frac{c^3}{b^3}\right) + 2Y\log\left(\frac{c}{a}\right) - p = 0, \tag{5.2}$$

where Y is the uniaxial yield stress [50]. Equation 5.2 was solved using MATHEMATICA, for a uniformly distributed pressure load of $30\,\text{dNmm}^{-2}$, and the radius of the plastic region was found to be $157.562\,\text{mm}$.

It is possible to derive the following equations [50]:

$$\sigma_{\theta\theta} = Y - \frac{2Y}{3}\left(1 - \frac{c^3}{b^3}\right) - 2Y\log\left(\frac{c}{r}\right) \qquad \text{for } a \leq r \leq c, \tag{5.3}$$

$$\sigma_{\theta\theta} = \frac{2Yc^3}{3b^3}\left(1 + \frac{b^3}{2r^3}\right) \qquad \text{for } c \leq r \leq b, \tag{5.4}$$

which describe the normal hoop stress $\sigma_{\theta\theta}$ as a function of the radius r.

The profile of the hoop stress can then be obtained from equations 5.3 and 5.4, where equation 5.3 describes the profile of the hoop stress in the plastic region and equation 5.4 describes the profile of the hoop stress in the elastic region.

5.4.2 Numerical analysis

This problem is also time independent and again the final solution is equivalent to that of an elasto-plastic analysis. Numerically the problem can be modelled in three dimensions, with the respective displacements fixed to zero in the respective symmetry planes. The spherical vessel is then reduced to an octant as illustrated in Figure 5.25(1). A number of meshes, of varying element density and type, were employed in the numerical analysis. Examples of meshes consisting of LT, BLP and TLH elements are illustrated in Figures 5.25(2), 5.25(3) and 5.25(4), respectively. The geometry of this problem requires a non-orthogonal mesh with regard to BLP and TLH elements as illustrated in Figures 5.25(3) and 5.25(4), respectively.
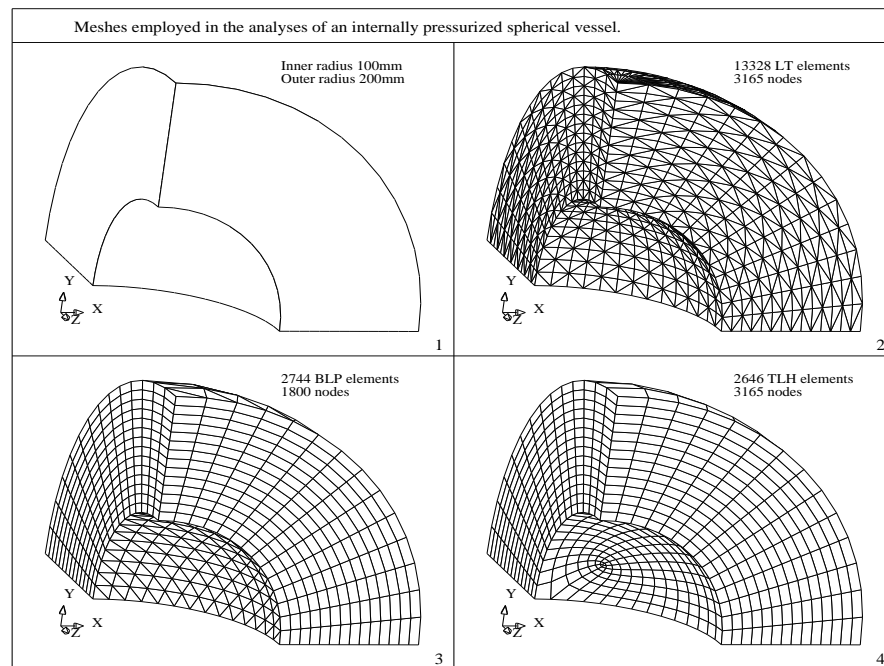
Figure 5.25: Meshes employed in the analyses of an internally pressurized spherical vessel.

5.4.3 Discussion of numerical results

Firstly, the problem was analysed with a series of meshes consisting of TLH elements. The meshes were continually refined. The hoop stress profiles, along the radii, as obtained from two of the numerical analyses are plotted and compared against the reference solution in Figures 5.26 and 5.27. In Figure 5.26 the results from one of the coarser meshes employed, consisting of 1,221 nodes and 950 TLH elements, are presented. Additionally, in Figure 5.27 the results from the finest mesh employed, consisting of 3,165 nodes and 2,646 TLH elements, are presented.

The close agreement of the FEM and the FVM is illustrated in both cases. However, it is important to note the closer agreement between the reference solution and the FVM in both cases. With regard to the FEM, the disagreement with the reference solution is worse for the coarser mesh.

These observations may be associated with the higher order, trilinear nature of the elements employed in the three dimensional analysis at this stage. With regard to the FVM, the implementation of surface tractions will involve bilinear face elements for TLH elements. Hence, when considering the application of surface tractions for the FEM and the FVM as described in equations 3.20 and 3.23, respectively, the contributions are different for the FVM and the FEM as a result of the different weighting techniques associated with each method.

Extending this point further, the weighting technique employed for the FVM may be more complementary, when applied generally, as all the terms are integrated conservatively at a local level. Conversely, for the FEM the weighting is not locally conservative which may introduce errors when surface tractions are employed. These conclusions are tentative and rely heavily on the authors own interpretation of the present observations, but they strongly suggest further possible avenues of research for the FVM, particularly with regard to surface tractions when associated with contact analysis.

It is important to note that the FVM employing the segregated displacement field approach (UVW) does not provide as favourable a comparison with regard to the reference solution. This can be attributed to the decoupling of the displacement components which is a direct consequence of the method. The decoupling will have greater effect when the problems are truly two or three dimensional and is also the case for elastic problems, as described in two dimensions by Fryer et al [43, 42].

Secondly, the problem was analysed with a series of meshes consisting of BLP elements. Again, the meshes were continually refined and the hoop stress profiles plotted in Figures 5.28 and 5.29.

There is much closer agreement between the FVM and the FEM for both the coarse mesh described in Figure 5.28 and the fine mesh described in Figure 5.29. This is attributable to the lower order, bilinear nature of the element concerned and the linear nature of the triangular faces over which the surface tractions are applied. As illustrated in Figure 5.25(3) the BLP elements are orientated so the pressure load (surface traction) is prescribed over a tri-

angular face. This was a fortuitous outcome of the automatic mesh generator employed [37] and it is obviously possible to further study the element when surface tractions are applied to the bilinear, quadrilateral faces, though it was not studied in this research.

Thirdly, the problem was analysed with a series of meshes consisting of LT elements. Again, the meshes were continually refined and the hoop stress profiles plotted in Figures 5.30 and 5.31.

As predicted in the previous Chapter, there is complete agreement between the FVM and the FEM with regard to LT elements. This is a consequence of the linear nature of both the element concerned and the triangular faces over which the surface traction is applied.

5.4.4 Algorithmic performance

As described in the previous section, this validation problem was solved in three dimensions with meshes consisting of a variety of element types and in each case an increasing number of elements.

Considering TLH elements, the FVM, employing a segregated algorithmic approach, and the FVM and the FEM, employing a standard algorithmic approach, were compared with regard to computational cost. The geometrical nature of this validation problem prohibits an orthogonally assembled mesh. Hence, for the standard FVM a BiCG solver is required due to the asymmetric nature of the coefficient matrix obtained. Conversely, for the standard FEM a CGM solver is sufficient as the coefficient matrix obtained is symmetric. These requirements agree with the conclusions of the previous Chapter. Additionally, for the segregated version of the FVM a GS (Gauss-Seidel) solver is applicable due to the diagonally dominant nature of the coefficient matrices obtained.

As illustrated in Figure 5.32, the segregated version of the FVM, employing the GS solver (UVW GS), requires considerably more CPU time than either the standard FVM (FVM BiCG) or the standard FEM (FEM CGM). As illustrated in Figure 5.33, the standard FVM, employing the BiCG solver (FVM BiCG) requires approximately twice the CPU time as

the FEM, employing the CGM solver (FEM CGM). This observation is expected due to the computational requirements of the two different linear solvers employed. Also with regard to TLH elements, the FVM visits twelve integration points per element, while the FEM visits eight Gauss points per element. Hence, any improvement in accuracy obtained by the FVM must be offset against the extra computational cost.

Considering BLP elements, the FEM (FEM CGM) and the FVM (FVM BiCG), employing the standard algorithmic approach, were compared with regard to computational cost, as illustrated in Figure 5.34. Again, the geometrical nature of the validation problem furnishes an asymmetric coefficient matrix with regard to the FVM and a symmetric coefficient matrix with regard to the FEM. Additionally, the FVM visits nine integration points per element, while the FEM visits six Gauss points per element.

Hence, the relative performances of the FVM and the FEM with regard to BLP elements are equivalent to those for TLH elements, as illustrated in Figures 5.34 and 5.33, respectively.

Considering TL elements, the FEM (FEM CGM) and the FVM (FVM CGM), employing the standard algorithmic approach, were compared with regard to computational cost, as illustrated in Figure 5.35. In this case the FVM and the FEM furnish identical, symmetric, coefficient matrices regardless of the problem geometry. However, the FVM visits six integration points, while the FEM visits a single Gauss point.

Hence, the FVM still incurs a greater computational cost, even when the same linear solver is employed, as illustrated in Figure 5.35.
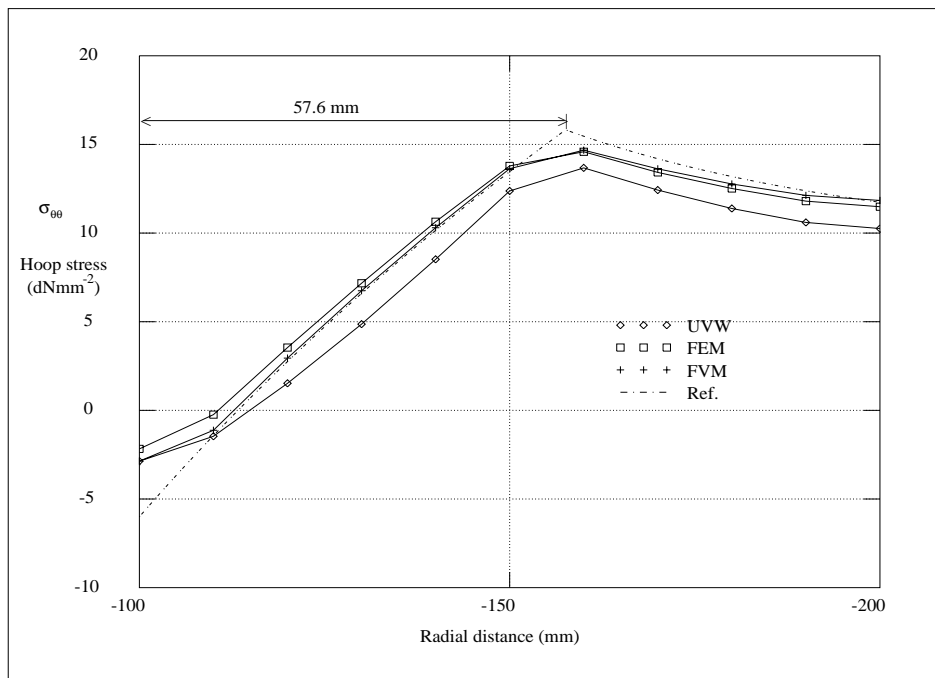
Figure 5.26: Mesh consisting of 1,221 nodes and 950 TLH elements.
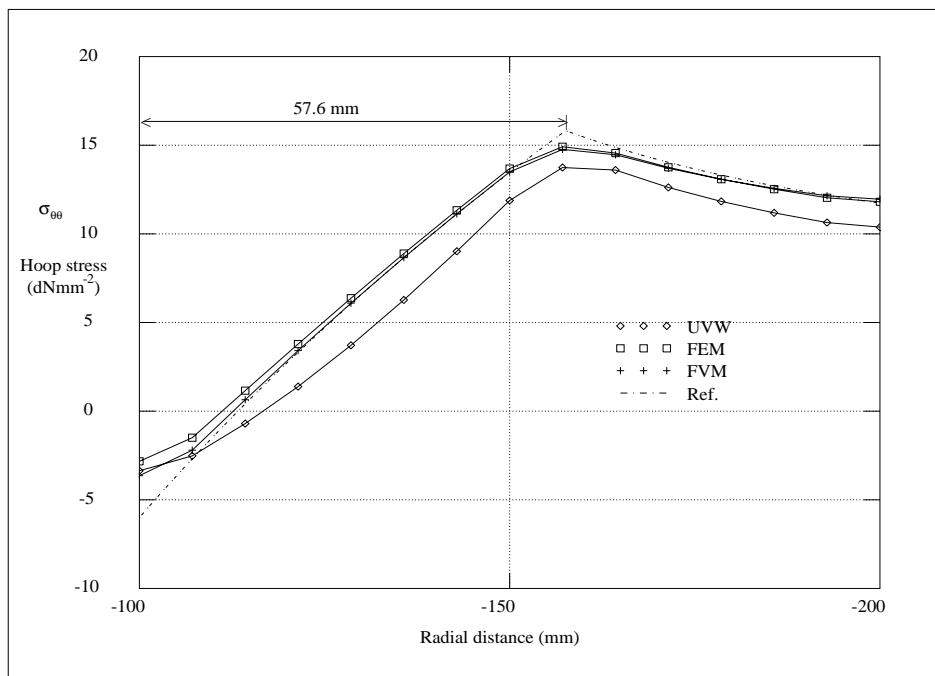
Figure 5.27: Mesh consisting of 3,165 nodes and 2,646 TLH elements.
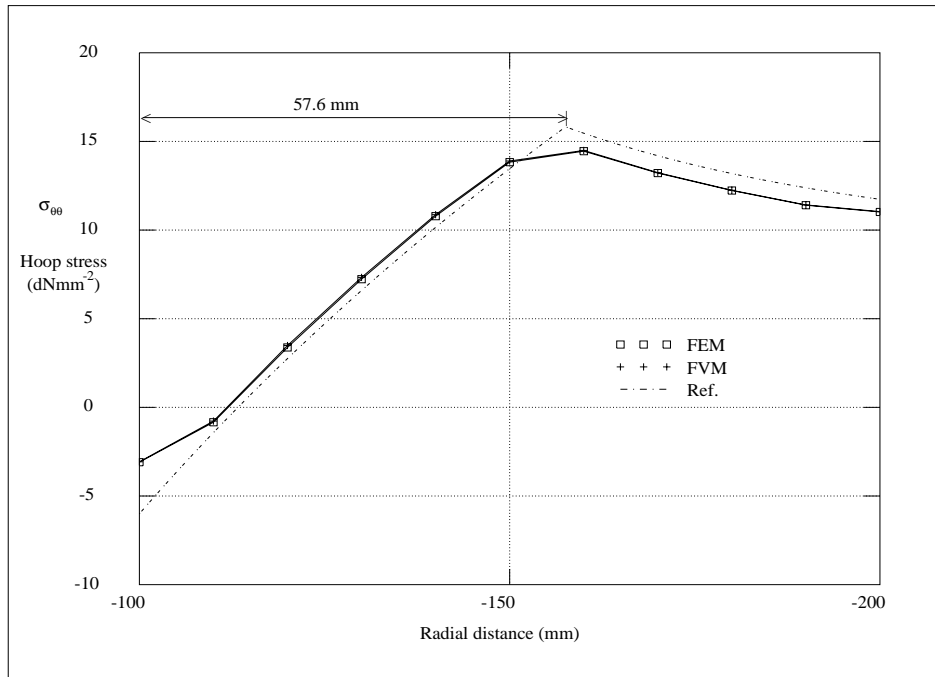
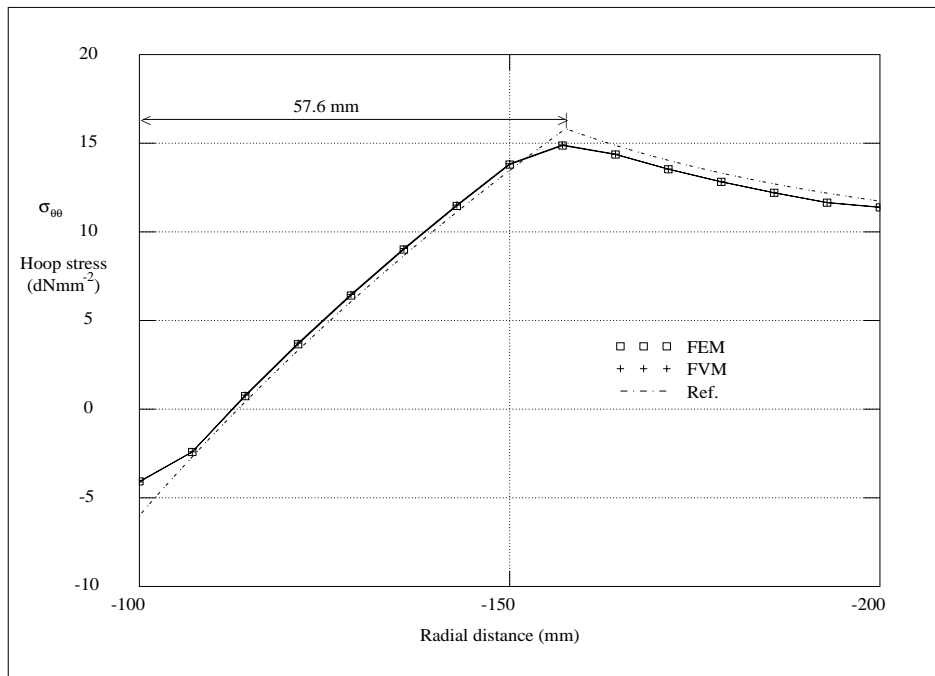Figure 5.28: Mesh consisting of 726 nodes and 1,000 BLP elements.

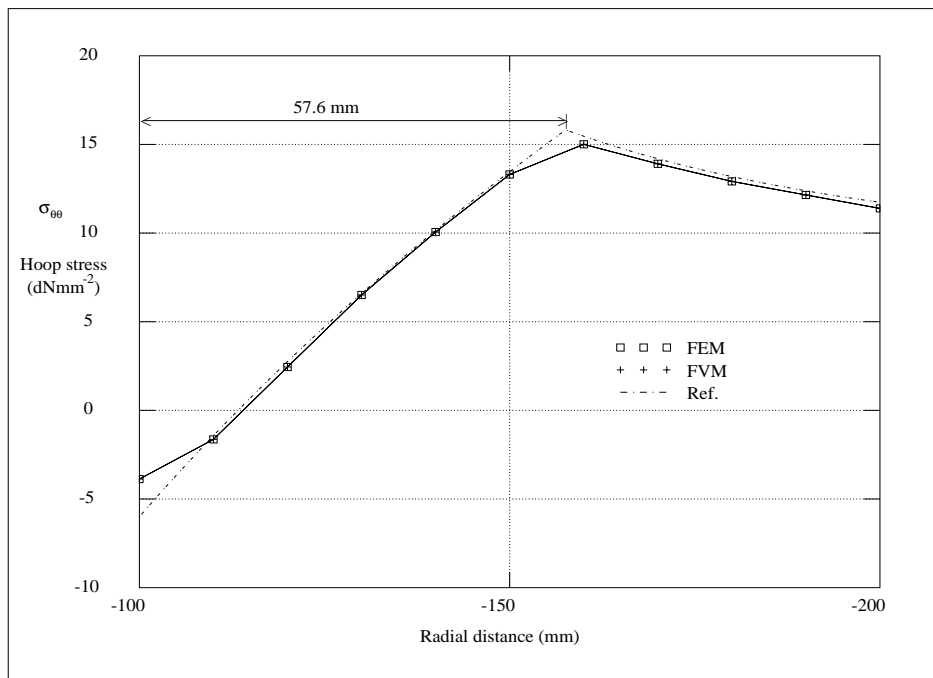Figure 5.29: Mesh consisting of 1,800 nodes and 2,744 BLP elements.

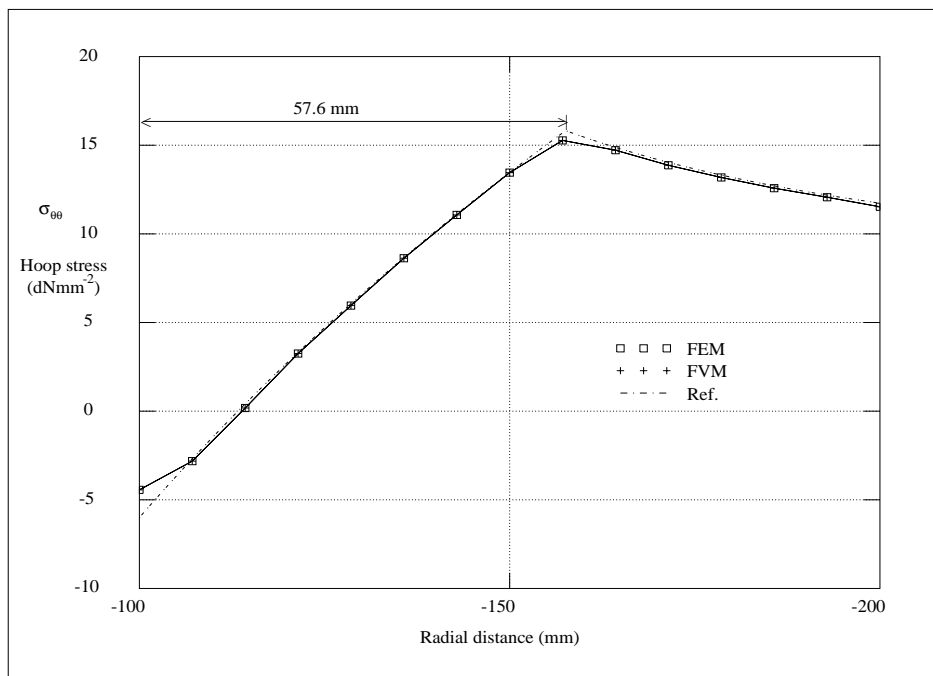Figure 5.30: Mesh consisting of 1,221 nodes and 4,800 LT elements.

Figure 5.31: Mesh consisting of 3,165 nodes and 13,328 LT elements.
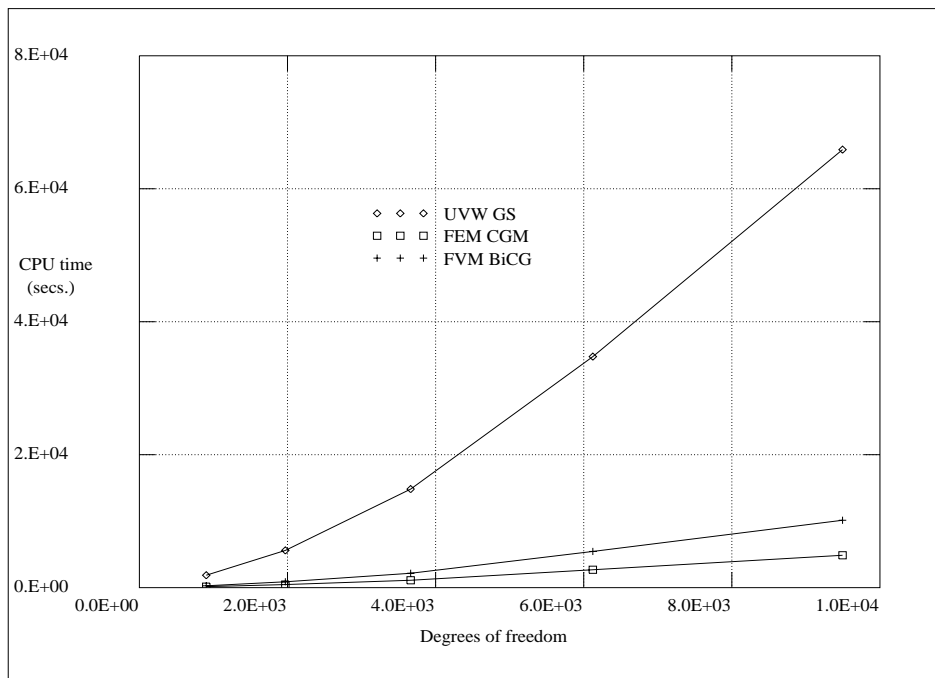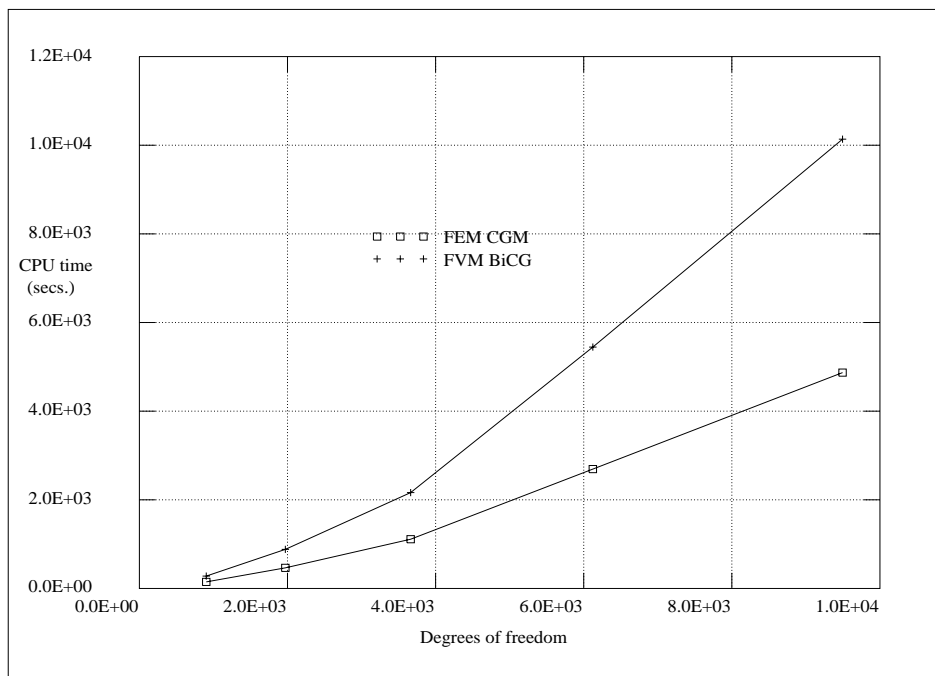
Figure 5.32: CPU times for TLH elements on a SPARC 4, 110MHz.

Figure 5.33: FE and FV CPU times for TLH elements on a SPARC 4, 110MHz.
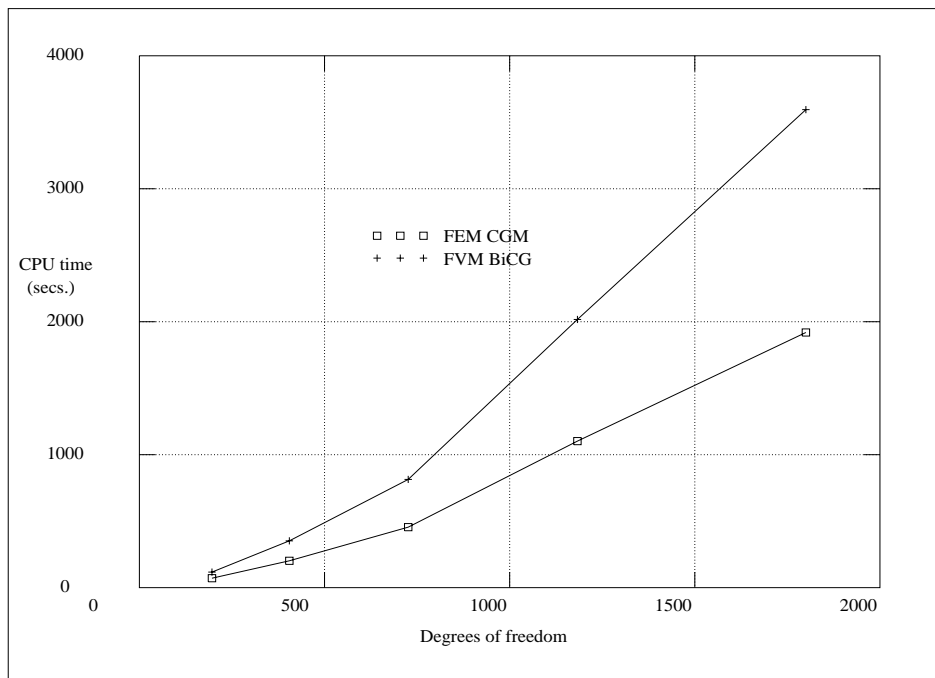
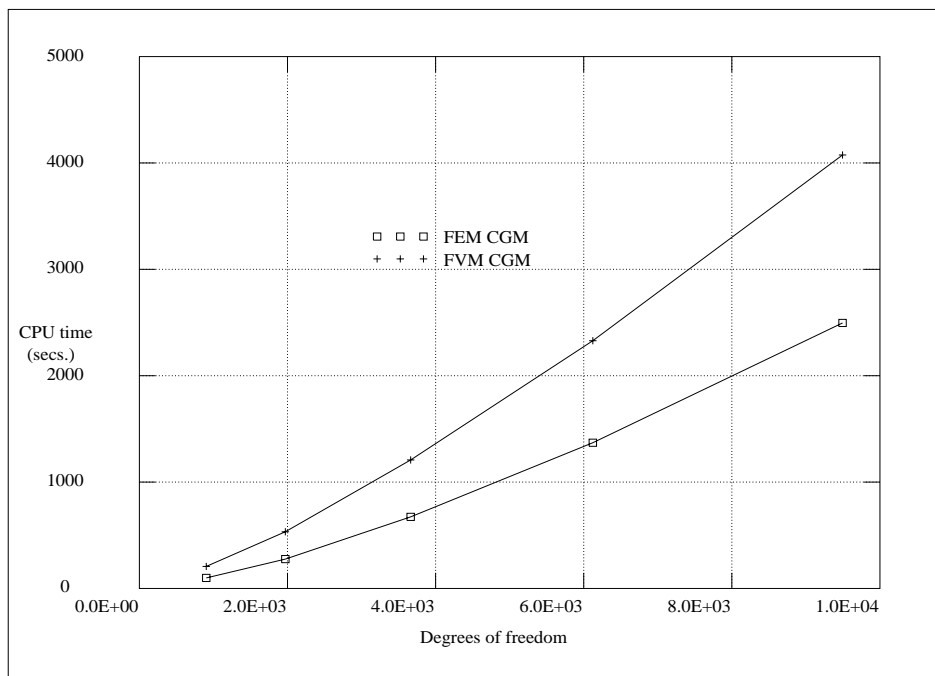Figure 5.34: CPU times for BLP elements on a SPARC 4, 110MHz.

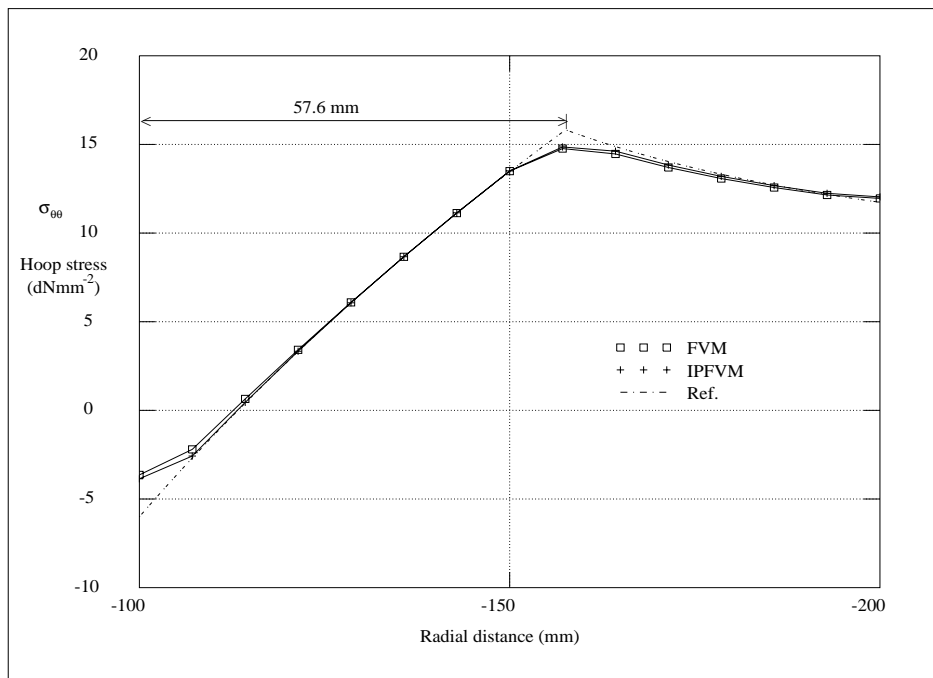Figure 5.35: CPU times for LT elements on a SPARC 4, 110MHz.

Figure 5.36: Comparison for FVM with TLH elements.
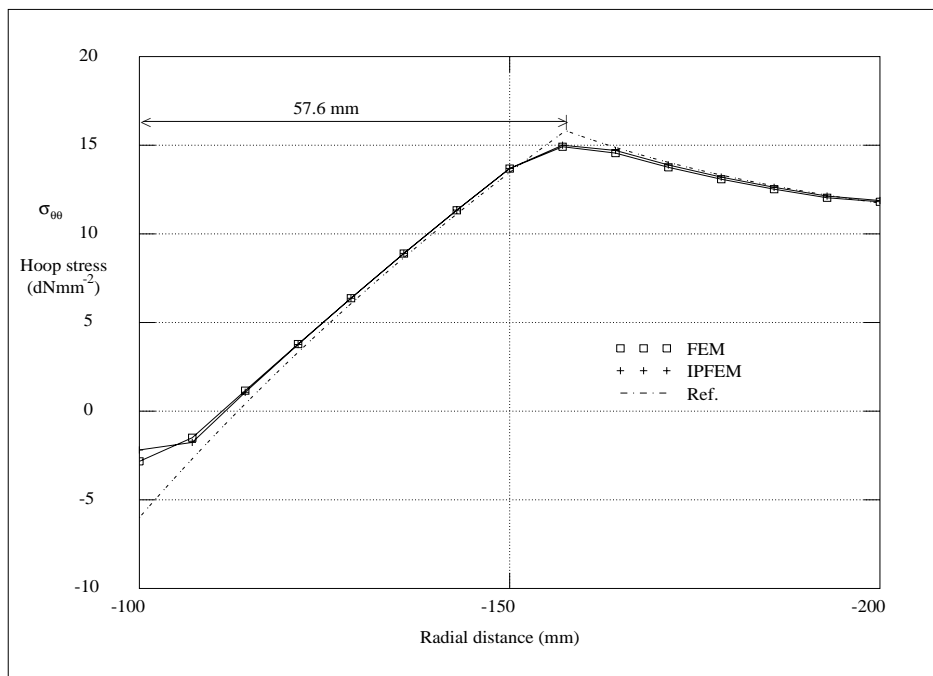

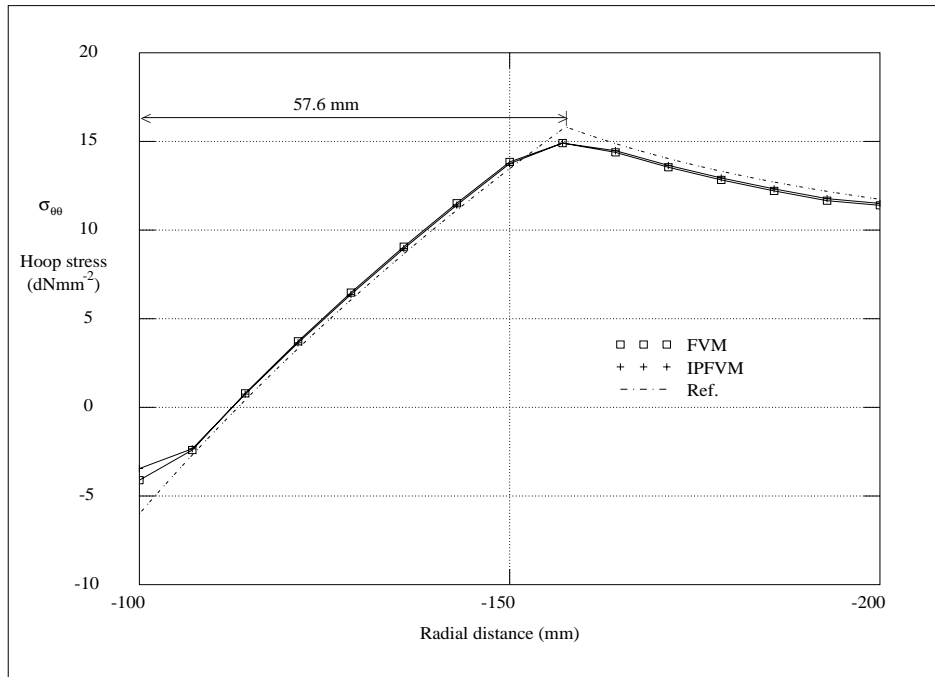Figure 5.37: Comparison for FEM with TLH elements.
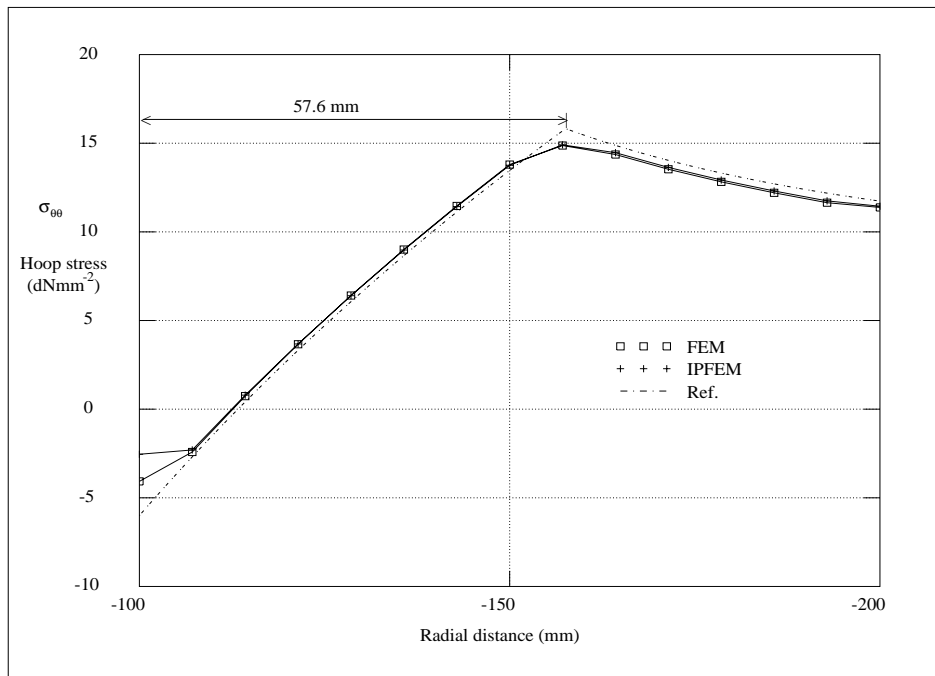
Figure 5.38: Comparison for FVM with BLP elements.

Figure 5.39: Comparison for FEM with BLP elements.

5.5 Closure

In this Chapter the FVM and the FEM have been compared against reference solutions for a variety of mechanical problems.

With regard to the linear elements in two and three dimensions the FVM and the FEM employed in this research are in complete agreement with respect to the numerical solution. The FVM requires slightly more computational effort as it visits more integration points than the FEM for an equivalent element.

It is important to note the potential superiority with regard to accuracy of the FVM when compared to the FEM with regard to the internally pressurised spherical vessel, when TLH elements are employed. However, it should also be noted that the resultant coefficient matrix associated with the FVM is asymmetric and requires approximately twice the computational effort to solve.